

# Rhombic skyrmion lattice coupled with orthorhombic structural distortion in $\text{EuAl}_4$

Masaki Gen,<sup>1,2,\*</sup> Rina Takagi,<sup>2,3,4,5</sup> Yoshito Watanabe,<sup>1</sup> Naofumi Matsuyama,<sup>6</sup> Yoshimitsu Kohama,<sup>6</sup> Akihiko Ikeda,<sup>7</sup> Yoshichika Ōnuki,<sup>2</sup> Takashi Kurumaji,<sup>1</sup> Taka-hisa Arima,<sup>1,2</sup> and Shinichiro Seki<sup>2,3,4</sup>

<sup>1</sup>Department of Advanced Materials Science, University of Tokyo, Kashiwa 277-8561, Japan

<sup>2</sup>RIKEN Center for Emergent Matter Science (CEMS), Wako 351-0198, Japan

<sup>3</sup>Institute of Engineering Innovation, University of Tokyo, Tokyo 113-0032, Japan

<sup>4</sup>Department of Applied Physics, University of Tokyo, Tokyo 113-8656, Japan

<sup>5</sup>PRESTO, Japan Science and Technology Agency (JST), Kawaguchi 332-0012, Japan

<sup>6</sup>Institute for Solid State Physics, University of Tokyo, Kashiwa 277-8581, Japan

<sup>7</sup>Department of Engineering Science, University of Electro-Communications, Chofu, Tokyo 182-8585, Japan

(Dated: September 27, 2022)

The centrosymmetric tetragonal itinerant magnet  $\text{EuAl}_4$  exhibits an intricate magnetic phase diagram including rhombic and square skyrmion-lattice (SkL) phases in the external magnetic field. Here, we report a dilatometric investigation on  $\text{EuAl}_4$  for three principal axes by means of the fiber-Bragg-grating technique, revealing anisotropic magnetostriction and magnetovolume effect associated with successive phase transitions. The rhombic and square SkL phases are found to possess  $\sim 0.10\%$  and  $\sim 0.03\%$  orthorhombic structural distortion within the  $ab$  plane, respectively. We propose that the coupling between the spin system and the lattice deformation should be essential for the structural instability in  $\text{EuAl}_4$ , yielding a rich variety of topological spin textures with spontaneous rotational-symmetry breaking as well as a potential controllability of the SkL phases by uniaxial stress or pressure.

Spontaneous rotational-symmetry breaking (SRSB) has long been a central issue in condensed-matter physics. A prominent recent topic is the electronic nematicity observed in heavy-fermion compounds [1], topological kagome metals [2], and copper/iron-based high- $T_c$  superconductors [3, 4], where the contribution of electron-phonon coupling has often been controversial. The SRSB is more widely seen with the onset of magnetic long-range order. In the presence of magnetic frustration, the mutual coupling of spin and lattice degrees of freedom can induce a magnetostructural transition with crystal symmetry lowering [5], as observed in solid oxygen [6, 7] and pyrochlore-based antiferromagnets [8, 9].

A magnetic skyrmion, a particlelike swirling spin texture, offers a fertile playground to explore emergent electromagnetic responses and transport properties [10–15]. In bulk crystals, skyrmions are usually arranged periodically, forming a skyrmion lattice with high rotational symmetry. In the framework of the Ginzburg–Landau theory, a triangular SkL, characterized by a triple- $\mathbf{Q}$  modulation with hexagonal symmetry, can be stabilized by the external magnetic field and entropy effect [16–18]. This was observed in a number of chiral [18–23] and polar magnets [24, 25] with the Dzyaloshinskii–Moriya (DM) interaction. Subsequently, the SkL was also discovered in rare-earth-based centrosymmetric itinerant magnets [26–30], whose magnetism is governed by the Ruderman–Kittel–Kasuya–Yosida (RKKY) interaction. Several mechanisms such as thermal fluctuations [31], higher-order multiple-spins interaction [32, 33], single-ion anisotropy [34–36], dipole–dipole interaction [37, 38], and interorbital frustration [39] are proposed as key ingredients for stabilizing the SkL in these compounds. It should be noted that the RKKY interaction is highly dependent on the shape of Fermi surface. In fact, skyrmions in a tetragonal magnet  $\text{GdRu}_2\text{Si}_2$  are arranged not in a triangular but a square lattice.

Recently, the SRSB of SkL was discovered in a binary intermetallic  $\text{EuAl}_4$  [30], which crystallizes in a centrosymmetric tetragonal structure (space group  $I4/mmm$ ) with a square lattice of localized spin-7/2  $\text{Eu}^{2+}$  ions. Figure 1(a) shows the magnetic-field-versus-temperature ( $H$ - $T$ ) phase diagram for  $H \parallel [001]$ , where seven magnetic phases (I–VII) appear as well as the paramagnetic (PM) and the forced ferromagnetic (FM) phases [30, 40]. In zero magnetic field, four magnetic transitions from the PM phase to phases VII, VI, V, and I take place at  $T_{N1} = 15.4$  K,  $T_{N2} = 13.2$  K,  $T_{N3} = 12.2$  K, and  $T_{N4} = 10.0$  K, respectively [30, 40–45]. The former two are of the second order, whereas the latter two are of the first order. A single crystal x-ray diffraction study revealed a tetragonal-to-orthorhombic structural transition with the  $B_{1g}$ -type distortion at  $T_{N3}$  [42]. When applying a magnetic field along [001], successive metamagnetic transitions from phase I to II, III, and IV take place below 5 K. Small-angle neutron and resonant x-ray scattering [30] unveiled the magnetic structures of all these phases; phases I and V are single- $\mathbf{Q}$  screw spiral with  $\mathbf{Q}_1 = (0.19, 0, 0)$  and  $(0.17, 0, 0)$ , respectively, II and III are double- $\mathbf{Q}$  SkL, IV and VII are double- $\mathbf{Q}$  vortex-antivortex lattice (VL), and VI is double- $\mathbf{Q}$  meron-antimeron lattice (ML). Two fundamental modulation vectors in phases III, VI, and VII are  $\mathbf{Q}_1 = (q, q, 0)$  and  $\mathbf{Q}_2 = (q, -q, 0)$ , where  $q \sim 0.085$ , so that the spin textures possess four-fold symmetry. In phases II and IV, on the other hand,  $\mathbf{Q}_1$  and  $\mathbf{Q}_2$  are tilted by  $\theta_q \sim 5^\circ$  toward the [100] direction, resulting in the rhombic SkL and VL, respectively [Fig. 1(b)]. In short, the SRSB is observed even in the double- $\mathbf{Q}$  states (II and IV) as well as in the single- $\mathbf{Q}$  states (I and V).

Theoretically, a *rectangular* SkL with four-fold symmetry breaking can appear on a square-lattice spin model by incorporating the competition among exchange interactions in momentum space  $J_{\mathbf{Q}}$  with  $\mathbf{Q}_1 = (q, q, 0)$ ,  $\mathbf{Q}_2 = (q, -q, 0)$ , and

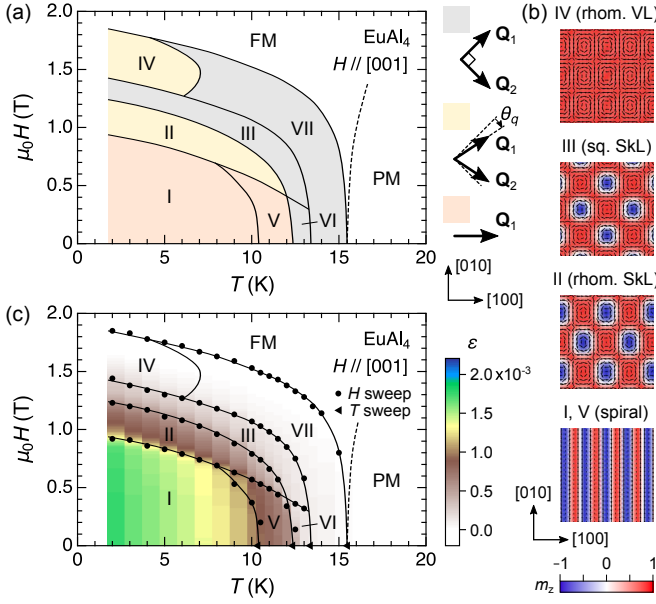


FIG. 1. (a)  $H$ - $T$  phase diagram of  $\text{EuAl}_4$  for  $H \parallel [001]$ , which is an excerpt from Refs. [30, 40] and reproduced in the present work. PM and FM represent paramagnetic and ferromagnetic phases, respectively. The fundamental modulation vectors in each phase are depicted in the right side. (b) Schematics of the real-space spin configurations in phases I~V. (c) Contour plots of the orthorhombic structural distortion  $\varepsilon = (b - a)/a_0$  mapped on the  $H$ - $T$  phase diagram revealed in this study.  $\varepsilon$  is set to zero at 0 T and 18 K. Closed circles (triangles) indicate transition fields (temperatures at 0 T) determined from peaks in  $\partial\varepsilon/\partial H$  ( $\partial\varepsilon/\partial T$ ). The phase boundary between phases IV and VII was not resolved in our magnetostriction measurements.

their higher harmonics,  $\mathbf{Q}_1 + \mathbf{Q}_2$  and  $\mathbf{Q}_1 - \mathbf{Q}_2$  [46, 47], though this picture is incompatible with the *rhombic* SkL in  $\text{EuAl}_4$ . Recalling the structural transition at  $T_{N3}$ , it is natural to anticipate that the spin-lattice coupling is responsible for stabilizing the rhombic double- $\mathbf{Q}$  modulation in phases II and IV. To shed light on this, it is important to clarify the in-field crystal-structure changes, which cannot be sensitively detected by x-ray or neutron studies. Dilatometry using the capacitance method has sufficient sensitivity, and a previous study [40] succeeded in observing the relative change in the lattice constant  $a$  on a detwinned crystal of  $\text{EuAl}_4$  while the information on the lattice constants  $b$  and  $c$  was lacking (we define  $a < b$  below  $T_{N3}$ ). Particularly, measurements of both  $a$  and  $b$  are essential to capture the magnitude of the  $B_{1g}$ -type distortion  $\varepsilon \equiv (b - a)/a_0$ .

In this work, we investigate the lattice constant changes for three principal axes associated with the field-induced phase transitions in  $\text{EuAl}_4$  using the fiber-Bragg-grating (FBG) technique, unveiling anisotropic magnetostriction and magneto-volume effect. Figure 1(c) shows a contour plot of  $\varepsilon$  mapped on the  $H$ - $T$  phase diagram: e.g.,  $\sim 0.10\%$  and  $\sim 0.03\%$  structural distortion is found in the rhombic and square SkL phases, respectively. Based on the microscopic consideration of a spin model, we argue that the spin-lattice coupling should act as the principal driving force for the multiple magnetostructural

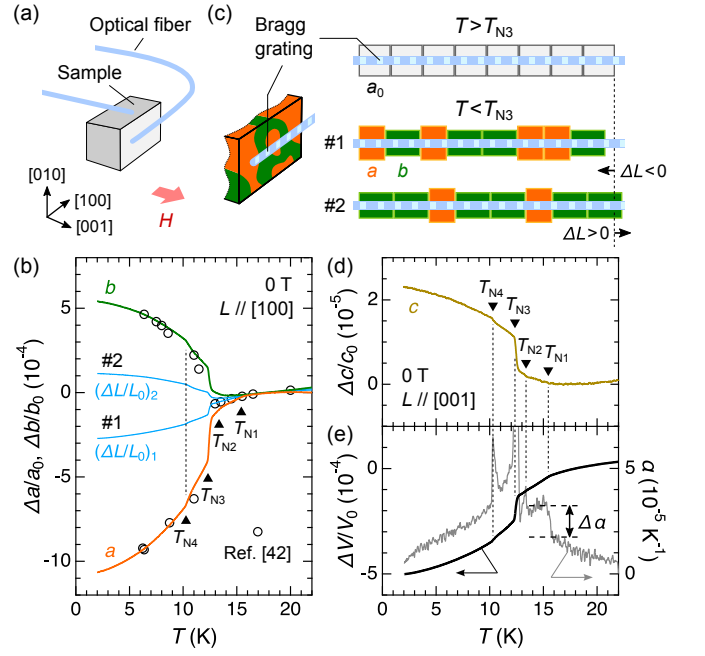


FIG. 2. (a) Schematic of the sample setting of FBG experiments, where  $\Delta L/L_0$  along [100] and [001] are simultaneously measured by adhering two optical fibers to one crystal orthogonally. (b) Thermal expansion measured along [100] in zero field (cyan lines):  $(\Delta L/L_0)_1$  [ $(\Delta L/L_0)_2$ ] for setting 1 (setting 2). Open circles are extracted from the lattice constants  $a$  and  $b$  reported in Ref. [42].  $\Delta a/a_0$  and  $\Delta b/b_0$  are calculated by  $(\Delta L/L_0)_1$ ,  $(\Delta L/L_0)_2$ , and the volume ratio of the magnetic domains  $(1 - p_i) : p_i$  with  $p_1 = 0.49$  ( $p_2 = 0.74$ ) for setting 1 (setting 2). (c) Schematic of the magnetic domains distribution in the (001) plane below  $T_{N3}$ . (d) Thermal expansion measured along [001] in zero field ( $\Delta c/c_0$ ). (e) Volume thermal expansion (left axis) and its temperature derivative (right axis) in zero field. All the thermal expansion data were obtained in the warming process.

transitions and the SRSB of SkL in  $\text{EuAl}_4$ .

The relative sample-length changes  $\Delta L/L_0$  along [100] and [001] were simultaneously measured, as illustrated in Fig. 2(a) (for experimental details, see Supplemental Material [48]). Throughout the paper, we define  $\Delta k$  ( $k = L, a, b, c$ ) as  $\Delta k \equiv k - k_0$  with the baseline value  $k_0$  at 0 T and 18 K and assume  $a_0 = b_0$ . The zero-field thermal expansion profiles measured along [100],  $(\Delta L/L_0)_1$  and  $(\Delta L/L_0)_2$ , which were taken under different sample settings, are shown by cyan lines in Fig. 2(b), along with the temperature evolution of  $\Delta a/a_0$  and  $\Delta b/b_0$  revealed by the previous x-ray diffraction study [42] (open circles). Opposite behaviors are observed between  $(\Delta L/L_0)_1$  and  $(\Delta L/L_0)_2$  below  $T_{N3}$ ; a positive thermal expansion for  $(\Delta L/L_0)_1$ , while negative for  $(\Delta L/L_0)_2$ . This discrepancy should be attributed to the difference in the magnetic domain patterns around the local area where the FBG was glued in each setting [Fig. 2(c)]. Assuming  $(\Delta L/L_0)_i = (1 - p_i)(\Delta a/a_0) + p_i(\Delta b/b_0)$ , we determine  $p_1 = 0.49$  for  $(\Delta L/L_0)_1$  and  $p_2 = 0.74$  for  $(\Delta L/L_0)_2$  so that they match the x-ray data at 6.3 K. Importantly,  $p_i$  is reproduced no matter how many times temperature or magnetic field is re-

peatedly scanned in our experiments (Fig. S2 [48]). Thanks to this feature, we can decompose  $\Delta a/a_0$  and  $\Delta b/b_0$  from the two experimental data sets  $(\Delta L/L_0)_1$  and  $(\Delta L/L_0)_2$  in the whole measured  $H$ - $T$  region using the following relations:  $\Delta a/a_0 = [p_2(\Delta L/L_0)_1 - p_1(\Delta L/L_0)_2]/(p_2 - p_1)$  and  $\Delta b/b_0 = [-(1 - p_2)(\Delta L/L_0)_1 + (1 - p_1)(\Delta L/L_0)_2]/(p_2 - p_1)$ . The calculated  $\Delta a/a_0$  and  $\Delta b/b_0$  as a function of temperature are shown by orange and green lines in Fig. 2(b), respectively, which agree well with the x-ray data.

As shown in Fig. 2(d), the observed  $\Delta L/L_0$  along [001], which corresponds to  $\Delta c/c_0$ , exhibits negative thermal expansion below  $T_{N1}$ . The entire change in  $\Delta c/c_0$  across the phase transitions is much smaller than those of  $\Delta a/a_0$  and  $\Delta b/b_0$ . This trend is in contrast to  $\text{GdRu}_2\text{Si}_2$  [53] and suggests the weak out-of-plane spin-lattice coupling in  $\text{EuAl}_4$ . We double check the reliability of our measurements by estimating thermodynamic quantities. Figure 2(e) shows the volume thermal expansion calculated as  $\Delta V/V_0 = \Delta a/a_0 + \Delta b/b_0 + \Delta c/c_0$  and its temperature derivative  $\alpha \equiv \partial(\Delta V/V_0)/\partial T$ .  $\alpha$  jumps by  $\Delta\alpha \approx -1.5 \times 10^{-4} \text{ K}^{-1}$  at  $T_{N1}$ . Adopting this value in combination with the reported specific heat change  $\Delta C_p \approx -6 \text{ J/(K}\cdot\text{mol)}$  at  $T_{N1}$  [40, 41] and the volume  $V \approx 107.1 \text{ \AA}^3/\text{f.u.}$  at 20 K [54] to the Ehrenfest relation  $\partial T_N/\partial p = T_N V (\Delta\alpha/\Delta C_p)$ , the pressure  $p$  dependence of  $T_{N1}$  is estimated to 2.5 K/GPa. This estimation agrees well with the previously obtained value  $\partial T_{N1}/\partial p = 2.24 \text{ K/GPa}$  [41].

Having confirmed the validity of our experimental and analytical methods from the thermal expansion data, we investigate the field-induced crystal-structure changes of  $\text{EuAl}_4$ . Figures 3(a)–3(c) show magnetostriction curves for  $H \parallel [001]$  measured at various temperatures. We obtain the field evolution of  $\Delta a/a_0$  and  $\Delta b/b_0$  by the same procedure described above (Fig. S1 [48]). As the magnetic field increases at 2 K,  $\Delta a/a_0$  monotonically increases accompanied by jumps at first-order transitions at  $H_{c1}$ ,  $H_{c2}$ , and  $H_{c3}$  in accord with Ref. [40]. In contrast,  $\Delta b/b_0$  and  $\Delta c/c_0$  monotonically decrease, indicating that the structural distortion associated with the magnetic ordering is gradually suppressed toward higher fields. Furthermore, we performed similar sets of thermal expansion and magnetostriction measurements for  $\Delta L/L_0 \parallel [100]$  on a crystal nearly detwinned by applying the thermal stress (Fig. S3 [48]); the observed  $\Delta L/L_0$  is closed to  $\Delta b/b_0$  and reasonably consistent with Figs. 2(b) and 3(a), while a uniaxial stress effect is seen in a shift of structural transition temperatures  $T_{N3}$  and  $T_{N4}$  by more than 1 K. The orthorhombic distortion  $\varepsilon$  calculated by  $\Delta b/b_0 - \Delta a/a_0$  is visualized on the  $H$ - $T$  phase diagram in Fig. 1(c). Note that  $\varepsilon$  may be slightly underestimated in high-field and high-temperature sides due to the missing incorporation of possible slight orthorhombic distortion at 0 T and 18 K [54] in our analysis (for details, see Supplemental Material [48]). The connection between the spin textures and orthorhombic structural distortion will be discussed later.

Our magnetostriction data provide insights on the pressure effect on the stability of the rhombic and square SkL phases. Figures 3(d) and 3(e) show magnetization and volume magnetostriction curves, respectively, for  $H \parallel [001]$  at 5 K. Here,

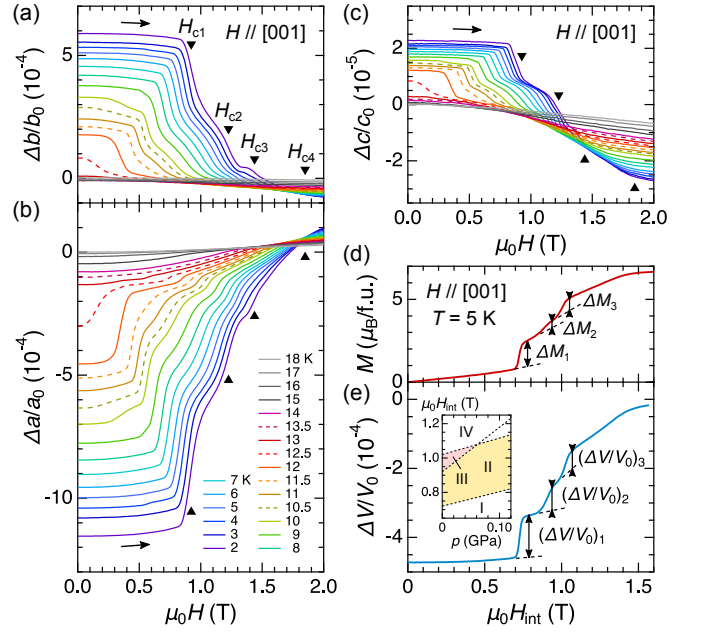


FIG. 3. [(a)–(c)] Magnetic-field evolution of the lattice constant changes (a)  $\Delta b/b_0$ , (b)  $\Delta a/a_0$ , and (c)  $\Delta c/c_0$  for  $H \parallel [001]$ . The color scale of temperature is shown in the inset of (b). Triangles denote magnetic transitions at 2 K. [(d) and (e)] (d) Magnetization and (e) volume magnetostriction curves for  $H \parallel [001]$  at 5 K. The horizontal axis  $H_{\text{int}}$  represents the magnetic field after demagnetization correction. The inset in (e) shows the thermodynamically predicted  $H$ - $p$  phase diagram. All the magnetostriction and magnetization data were obtained in the field-increasing process.

the demagnetization is corrected so as to accurately estimate the magnitudes of the magnetization jumps at  $H_{c1}$ ,  $H_{c2}$ , and  $H_{c3}$ :  $\Delta M_1 \approx 1.6 \mu_B/\text{f.u.}$ ,  $\Delta M_2 \approx 0.3 \mu_B/\text{f.u.}$ , and  $\Delta M_3 \approx 0.6 \mu_B/\text{f.u.}$ , respectively. The corresponding volume jumps are  $(\Delta V/V_0)_1 \approx 1.2 \times 10^{-4}$ ,  $(\Delta V/V_0)_2 \approx 0.7 \times 10^{-4}$ , and  $(\Delta V/V_0)_3 \approx 0.5 \times 10^{-4}$ , respectively. According to Clausius–Clapeyron’s equation  $\partial(\mu_0 H_c)/\partial p = \Delta V/\Delta M$ , the pressure dependence of each critical field is estimated to  $\partial(\mu_0 H_{c1})/\partial p \approx 0.8 \text{ T/GPa}$ ,  $\partial(\mu_0 H_{c2})/\partial p \approx 2.6 \text{ T/GPa}$ , and  $\partial(\mu_0 H_{c3})/\partial p \approx 1.0 \text{ T/GPa}$ . A relatively large value of  $\partial(\mu_0 H_{c2})/\partial p$  is attributed to the substantial volume expansion at the transition to phase III in spite of the small magnetization jump. The predicted  $H$ - $p$  phase diagram is shown in the inset of Fig. 3(e), suggesting that the square SkL can be annihilated by applying hydrostatic pressure lower than 0.1 GPa. The stability of each SkL phase may also be controllable by tuning the chemical pressure such as the isovalent Ga substitution for Al [55]. Indeed, the  $H$ - $T$  phase diagrams of  $\text{EuGa}_4$  and  $\text{EuGa}_2\text{Al}_2$  are simpler than that of  $\text{EuAl}_4$  [56, 57], presumably suggesting the absence of orthorhombic structural distortion and the rhombic SkL phase in these compounds. A systematic investigation on the phase diagram of  $\text{Eu}(\text{Ga}_{1-x}\text{Al}_x)_4$  system would be intriguing.

To understand the magnetic instability in  $\text{EuAl}_4$ , we start from the classical Heisenberg model on a simple square lattice:  $\mathcal{H} = \sum_{\langle i,j \rangle k} J_k \mathbf{S}_i \cdot \mathbf{S}_j + \mathcal{H}_{\text{ex}}$ , where  $J_1 < 0$ ,  $J_2 > 0$ , and

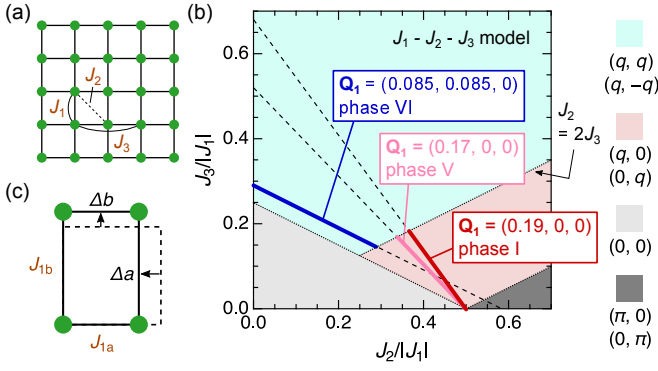


FIG. 4. (a) Exchange interactions up to the third NN on a square lattice. (b) Exchange parameter sets of  $J_2$  and  $J_3$  consistent with the fundamental  $\mathbf{Q}$  vectors for phases VI, V, and I in zero field. The phase diagram is an excerpt from Ref. [58] (see text for details). (c) Tetragonal-to-orthorhombic distortion on a square lattice, resulting in inequivalent NN exchanges  $J_{1a} \approx J_1[1 + (dJ_1/dr)\Delta a]$  and  $J_{1b} \approx J_1[1 + (dJ_1/dr)\Delta b]$ .

$J_3 > 0$  are the exchange interactions up to the third nearest neighbor (NN) [Fig. 4(a)] and  $\mathcal{H}_{\text{ex}}$  includes extra terms. This model can host various kinds of single- $\mathbf{Q}$  and multiple- $\mathbf{Q}$  spin textures depending on  $\mathcal{H}_{\text{ex}}$ ; e.g., the double- $\mathbf{Q}$  ML is stabilized in the presence of the single-ion anisotropy and compass anisotropy [58], which would be relevant to phase VI in  $\text{EuAl}_4$  [30]. If we neglect  $\mathcal{H}_{\text{ex}}$ , incommensurate ordering vectors  $\mathbf{Q} = (\pm q, \pm q, 0)$  with  $q = \arccos(-\frac{J_1}{2J_2+4J_3})$  are selected for  $2J_3 > J_2$  whereas  $\mathbf{Q} = (\pm q, 0, 0)$  or  $(0, \pm q, 0)$  with  $q = \arccos(-\frac{J_1+2J_2}{4J_3})$  for  $J_2 > 2J_3$  [58]. The exchange parameter sets that agree with the  $\mathbf{Q}$  vectors for the zero-field phases VI, V, and I [30, 44] are plotted in a parameter space of  $J_2/|J_1|$  and  $J_3/|J_1|$  in Fig. 4(b). As phases VI, V, and I should compete with each other within a small energy scale,  $(J_2/|J_1|, J_3/|J_1|) \approx (0.3, 0.15)$  is a reasonable parameter position for  $\text{EuAl}_4$ . We note that the  $\mathbf{Q}$  switching at  $T_{N3}$  and  $T_{N4}$  cannot occur within the frozen  $J_1$ - $J_2$ - $J_3$  model.

We here propose the spin-lattice coupling as a driving force to modify the  $J$ 's through a magnetostructural transition. This mechanism is reasonable to consider in  $\text{EuAl}_4$  on the basis of the observed exceptionally large thermal expansion and magnetostriction associated with the magnetic transitions ( $\sim 10^{-3}$ ) compared to those in other SkL-hosting Eu/Gd-based itinerant magnets ( $10^{-4} \sim 10^{-5}$ ) [53, 59, 60]. This collective phenomenon is known as the spin Jahn-Teller effect, where the magnetic frustration is relieved by favoring one of the competing exchange interactions through the lattice distortion [5]. The  $B_{1g}$ -type distortion is selected for the transition from phase VI to V at  $T_{N3}$  [42], indicating that the FM  $J_1$  along the  $a$  and  $b$  axes become inequivalent:  $J_{1a} \approx J_1[1 + (dJ_1/dr)\Delta a]$  and  $J_{1b} \approx J_1[1 + (dJ_1/dr)\Delta b]$ , respectively [Fig. 4(c)]. If  $dJ_1/dr > 0$ ,  $J_{1b}$  is favored whereas  $J_{1a}$  is disfavored, so that the  $\mathbf{Q}$  vector should be oriented along the  $a$  axis [61]. This picture is compatible with the  $\mathbf{Q}$  switching from  $(0.085, 0.085, 0)$  to  $(0.17, 0, 0)$  at  $T_{N3}$  because the total exchange energy can be reduced for the latter. The additional first-order transition

from phase V to I at  $T_{N4}$ , which accompanies a modulation-period change from  $q = 0.17$  to  $0.19$  while conserving the orientation of the  $\mathbf{Q}$  vector, suggests the competition of these two spiral states in the presence of the spin-lattice coupling; phase I is eventually stabilized as a ground state by enhancing the orthorhombic structural distortion  $\varepsilon \sim 1.6 \times 10^{-3}$  and consequently increasing  $J_2/|J_{1a}|$  (or  $J_2/|J_{1b}|$ ). We note that a uniaxial stress should facilitate the magnetostructural transitions at  $T_{N3}$  and  $T_{N4}$  because the system can save the elastic energy, which is indeed observed as mentioned above (Fig. S3 [48]).

The importance of the spin-lattice coupling is also corroborated from the strong correlation between the in-field spin textures and orthorhombic structural distortion. In the rhombic SkL phase (II), two fundamental  $\mathbf{Q}$  vectors are tilted from  $\mathbf{Q}_1 = (q, q, 0)$  and  $\mathbf{Q}_2 = (q, -q, 0)$  ( $q \sim 0.085$ ) by  $\theta_q \sim 5^\circ$  [30]. As can be seen from Fig. 1(c), a large structural distortion  $\varepsilon \sim 1.0 \times 10^{-3}$  exists in phase II like in phase V, suggesting the importance of the spin-lattice coupling for the rhombic  $\mathbf{Q}$  modulation. A discontinuous drop of  $\theta_q$  to zero at the SkL-SkL transition from phase II to III [30] is also a remarkable feature supporting this scenario. The fundamental modulations  $\mathbf{Q}_1 = (0.083, 0.083, 0)$  and  $\mathbf{Q}_2 = (0.083, -0.083, 0)$  in the square SkL phase (III) are almost identical with those in the zero-field phase VI [30, 44]. However, a moderate structural distortion  $\varepsilon \sim 3 \times 10^{-4}$  is found in phase III [Fig. 1(c)], indicating that  $J_{1a}$  and  $J_{1b}$  remain inequivalent. Such a deviation from the tetragonal symmetry in phase III was not observed in the previous quantum beam experiments potentially due to insufficient resolution [30]. Interestingly, a reentrant symmetry breaking of the spin texture is seen in the high-field rhombic VL phase (IV) [30], though the orthorhombic structural distortion seems monotonically suppressed toward higher fields [Fig. 1(c)]. The reason why the VL is more prone to deformation (in terms of spin textures) than the SkL is elusive at this stage. A theoretical framework incorporating local phonon modes or inequivalent  $J_{1a}$  and  $J_{1b}$  on the square lattice would be a promising approach to reproduce versatile magnetic phases in  $\text{EuAl}_4$ , which is left for future work.

In summary, we have comprehensively revealed the crystal-structure changes of  $\text{EuAl}_4$  associated with the field-induced phase transitions to address the microscopic origin of the SRSB of the SkL. The amplitudes of the orthorhombic structural distortion are quantitatively estimated for each magnetic phase. The appearance of two types of SkL phases should originate from the magnetic frustration in momentum space coupled with the lattice degrees of freedom. Furthermore, the orthorhombic structural distortion accompanies a pronounced magnetovolume effect.  $\text{EuAl}_4$  would be an ideal playground to explore the tunability of the SkL phases by pressure as well as uniaxial stress.

The authors appreciate S. Hayami and H. Yoshimochi for fruitful discussions. The authors appreciate S. Shimomura for providing the data of the lattice constants of  $\text{EuAl}_4$  in Ref. [42]. This work was financially supported by the JSPS KAKENHI Grants-In-Aid for Scientific Research (No.

19H01835, No. 19H05826, and No. 20J10988). M.G. was a postdoctoral research fellow of the JSPS.

\* [masaki.gen@riken.jp](mailto:masaki.gen@riken.jp)

- [1] R. Okazaki, T. Shibauchi, H. J. Shi, Y. Haga, T. D. Matsuda, E. Yamamoto, Y. Onuki, H. Ikeda, and Y. Matsuda, Rotational symmetry breaking in the hidden-order phase of URu<sub>2</sub>Si<sub>2</sub>, *Science* **331**, 439 (2011).
- [2] L. Nie, K. Sun, W. Ma, D. Song, L. Zheng, Z. Liang, P. Wu, F. Yu, J. Li, M. Shan, D. Zhao, S. Li, B. Kang, Z. Wu, Y. Zhou, K. Liu, Z. Xiang, J. Ying, Z. Wang, T. Wu, and X. Chen, Charge-density-wave-driven electronic nematicity in a kagome superconductor, *Nature* **604**, 59 (2022).
- [3] M. J. Lawler, K. Fujita, J. Lee, A. R. Schmidt, Y. Kohsaka, C. K. Kim, H. Eisaki, S. Uchida, J. C. Davis, J. P. Sethna, and E.-A. Kim, Intra-unit-cell electronic nematicity of the high- $T_c$  copper-oxide pseudogap states, *Nature* **466**, 347 (2010).
- [4] S. Kasahara, H. J. Shi, K. Hashimoto, S. Tonegawa, Y. Mizukami, T. Shibauchi, K. Sugimoto, T. Fukuda, T. Terashima, A. H. Nevidomskyy, and Y. Matsuda, *Nature* **486**, 382 (2012).
- [5] C. Lacroix, P. Mendels, and F. Mila, *Introduction to Frustrated Magnetism*, Heidelberg: Springer, 2011.
- [6] G. C. De Fotis, Magnetism of solid oxygen, *Phys. Rev. B* **23**, 4714 (1981).
- [7] P. W. Stephens and C. F. Majkrzak, Magnetic structure and dynamics in the  $\alpha$  and  $\beta$  phases of solid oxygen, *Phys. Rev. B* **33**, 1 (1986).
- [8] S.-H. Lee, C. Broholm, T. H. Kim, W. Ratcliff II, and S.-W. Cheong, Local Spin Resonance and Spin-Peierls-like Phase Transition in a Geometrically Frustrated Antiferromagnet, *Phys. Rev. Lett.* **84**, 3718 (2000).
- [9] M. Matsuda, H. Ueda, A. Kikkawa, Y. Tanaka, K. Katsumata, Y. Narumi, T. Inami, Y. Ueda, and S.-H. Lee, Spin-lattice instability to a fractional magnetization state in the spinel HgCr<sub>2</sub>O<sub>4</sub>, *Nat. Phys.* **3**, 397 (2007).
- [10] A. Neubauer, C. Pfleiderer, B. Binz, A. Rosch, R. Ritz, P. G. Niklowitz, and P. Böni, Topological Hall Effect in the A Phase of MnSi, *Phys. Rev. Lett.* **102**, 186602 (2009).
- [11] F. Jonietz, S. Mühlbauer, C. Pfleiderer, A. Neubauer, W. Münzer, A. Bauer, T. Adams, R. Georgii, P. Böni, R. A. Duine, K. Everschor, M. Garst, and A. Rosch, Spin Transfer Torques in MnSi at Ultralow Current Densities, *Science* **330**, 1648 (2010).
- [12] T. Schulz, R. Ritz, A. Bauer, M. Halder, M. Wagner, C. Franz, C. Pfleiderer, K. Everschor, M. Garst, and A. Rosch, Emergent electrodynamics of skyrmions in a chiral magnet, *Nat. Phys.* **8**, 301 (2012).
- [13] P.-J. Hsu, A. Kubetzka, A. Finco, N. Romming, K. von Bergmann, and R. Wiesendanger, Electric-field-driven switching of individual magnetic skyrmions, *Nat. Nanotech.* **12**, 123 (2017).
- [14] M. Hirschberger, L. Spitz, T. Nomoto, T. Kurumaji, S. Gao, J. Masell, T. Nakajima, A. Kikkawa, Y. Yamasaki, H. Sagayama, H. Nakao, Y. Taguchi, R. Arita, T. Arima, and Y. Tokura, Topological Nernst Effect of the Two-Dimensional Skyrmion Lattice, *Phys. Rev. Lett.* **125**, 076602 (2020).
- [15] M. Akazawa, H.-Y. Lee, H. Takeda, Y. Fujima, Y. Tokunaga, T. Arima, J. H. Han, and M. Yamashita, Topological Thermal Hall Effect Induced by Magnetic Skyrmions, arXiv:2102.06430.
- [16] A. N. Bogdanov and D. A. Yablonskii, Thermodynamically Stable “Vortices” in Magnetically Ordered Crystals. The Mixed State of Magnets, *Sov. Phys. JETP* **68**, 101 (1989).
- [17] A. Bogdanov and A. Hubert, Thermodynamically Stable Magnetic Vortex States in Magnetic Crystals, *J. Magn. Magn. Mater.* **138**, 255 (1994).
- [18] S. Mühlbauer, B. Binz, F. Jonietz, C. Pfleiderer, A. Rosch, A. Neubauer, R. Georgii, and P. Böni, Skyrmion Lattice in a Chiral Magnet, *Science* **323**, 915 (2009).
- [19] X. Z. Yu, Y. Onose, N. Kanazawa, J. H. Park, J. H. Han, Y. Matsui, N. Nagaosa, Y. Tokura, Real-space observation of a two-dimensional skyrmion crystal, *Nature* **465**, 901 (2010).
- [20] X. Z. Yu, N. Kanazawa, Y. Onose, K. Kimoto, W. Z. Zhang, S. Ishiwata, Y. Matsui, and Y. Tokura, Near room-temperature formation of a skyrmion crystal in thin-films of the helimagnet FeGe, *Nat. Mater.* **10**, 106 (2011).
- [21] S. Seki, X. Z. Yu, S. Ishiwata, and Y. Tokura, Observation of Skyrmions in a Multiferroic Material, *Science* **336**, 198 (2012).
- [22] Y. Tokunaga, X. Z. Yu, J. S. White, H. M. Rønnow, D. Morikawa, Y. Taguchi, Y. Tokura, A new class of chiral materials hosting magnetic skyrmions beyond room temperature, *Nat. Commun.* **6**, 7638 (2015).
- [23] K. Kaneko, M. D. Frontzek, M. Matsuda, A. Nakao, K. Munakata, T. Ohhara, M. Kakihana, Y. Haga, M. Hedo, T. Nakama, and Y. Onuki, Unique Helical Magnetic Order and Field-Induced Phase in Trillium Lattice Antiferromagnet EuPtSi, *J. Phys. Soc. Jpn.* **88**, 013702 (2019).
- [24] I. Kézsmárki, S. Bordács, P. Milde, E. Neuber, L. M. Eng, J. S. White, H. M. Rønnow, C. D. Dewhurst, M. Mochizuki, K. Yanai, H. Nakamura, D. Ehlers, V. Tsurkan and A. Loidl, Néel-type skyrmion lattice with confined orientation in the polar magnetic semiconductor GaV<sub>4</sub>S<sub>8</sub>, *Nat. Mater.* **14**, 1116 (2015).
- [25] T. Kurumaji, T. Nakajima, V. Ukleev, A. Feoktystov, T. Arima, K. Kakurai, and Y. Tokura, Néel-Type Skyrmion Lattice in the Tetragonal Polar Magnet VOSe<sub>2</sub>O<sub>5</sub>, *Phys. Rev. Lett.* **119**, 237201 (2017).
- [26] T. Kurumaji, T. Nakajima, M. Hirschberger, A. Kikkawa, Y. Yamasaki, H. Sagayama, H. Nakao, Y. Taguchi, T. Arima, and Y. Tokura, Skyrmion lattice with a giant topological Hall effect in a frustrated triangular-lattice magnet, *Science* **365**, 914 (2019).
- [27] M. Hirschberger, T. Nakajima, S. Gao, L. Peng, A. Kikkawa, T. Kurumaji, M. Kriener, Y. Yamasaki, H. Sagayama, H. Nakao, K. Ohishi, K. Kakurai, Y. Taguchi, X. Z. Yu, T. Arima, and Y. Tokura, Skyrmion phase and competing magnetic orders on a breathing kagomé lattice, *Nat. Commun.* **10**, 5831 (2019).
- [28] N. D. Khanh, T. Nakajima, X. Z. Yu, S. Gao, K. Shibata, M. Hirschberger, Y. Yamasaki, H. Sagayama, H. Nakao, L. Peng, K. Nakajima, R. Takagi, T. Arima, Y. Tokura, and S. Seki, Nanometric square skyrmion lattice in a centrosymmetric tetragonal magnet, *Nat. Nanotech.* **15**, 444 (2020).
- [29] N. D. Khanh, T. Nakajima, S. Hayami, S. Gao, Y. Yamasaki, H. Sagayama, H. Nakao, R. Takagi, Y. Motome, Y. Tokura, T. Arima, and S. Seki, Zoology of Multiple- $Q$  Spin Textures in a Centrosymmetric Tetragonal Magnet with Itinerant Electrons, *Adv. Sci.* **2**, 105254 (2022).
- [30] R. Takagi, N. Matsuyama, V. Ukleev, L. Yu, J. S. White, S. Francoual, J. R. L. Mardegan, S. Hayami, H. Saito, K. Kaneko, K. Ohishi, Y. Ōnuki, T. Arima, Y. Tokura, T. Nakajima, and S. Seki, *Nat. Commun.* **13**, 1472 (2022).
- [31] T. Okubo, S. Chung, and H. Kawamura, Multiple- $q$  States and the Skyrmion Lattice of the Triangular-Lattice Heisenberg Antiferromagnet under Magnetic Fields, *Phys. Rev. Lett.* **108**, 017206 (2012).
- [32] R. Ozawa, S. Hayami, and Y. Motome, Zero-Field Skyrmions with a High Topological Number in Itinerant Magnets, *Phys.*

- Rev. Lett. **118**, 147205 (2017).
- [33] S. Hayami, R. Ozawa, and Y. Motome, Effective bilinear-biquadratic model for noncoplanar ordering in itinerant magnet, Phys. Rev. B **95**, 224424 (2017).
- [34] A. O. Leonov and M. Mostovoy, Multiply periodic states and isolated skyrmions in an anisotropic frustrated magnet, Nat. Commun. **6**, 8275 (2015).
- [35] S. Hayami and Y. Motome, Effect of magnetic anisotropy on skyrmions with a high topological number in itinerant magnets, Phys. Rev. B **99**, 094420 (2019).
- [36] Z. Wang, Y. Su, S.-Z. Lin, and C. D. Batista, Skyrmion Crystal from RKKY Interaction Mediated by 2D Electron Gas, Phys. Rev. Lett. **124**, 207201 (2020).
- [37] O. I. Utesov, Thermodynamically stable skyrmion lattice in a tetragonal frustrated antiferromagnet with dipolar interaction, Phys. Rev. B **103**, 064414 (2021).
- [38] J. A. M. Paddison, B. K. Rai, A. F. May, S. A. Calder, M. B. Stone, M. D. Frontzek, A. D. Christianson, Magnetic Interactions of the Centrosymmetric Skyrmion Material  $\text{Gd}_2\text{PdSi}_3$ , arXiv:2203.00066.
- [39] T. Nomoto, T. Koretsune, and R. Arita, Formation Mechanism of the Helical  $Q$  Structure in Gd-Based Skyrmion Materials, Phys. Rev. Lett. **125**, 117204 (2020).
- [40] W. R. Meier, J. R. Torres, R. P. Hermann, J. Zhao, B. Lavina, B. C. Sales, and A. F. May, Thermodynamic insights into the intricate magnetic phase diagram of  $\text{EuAl}_4$ , Phys. Rev. B **106**, 094421 (2022).
- [41] A. Nakamura, T. Uejo, F. Honda, T. Takeuchi, H. Harima, E. Yamamoto, Y. Hag, K. Matsubayashi, Y. Uwatoko, M. Hedo, T. Nakama, and Y. Ōnuki, Transport and Magnetic Properties of  $\text{EuAl}_4$  and  $\text{EuGa}_4$ , J. Phys. Soc. Jpn. **84**, 124711 (2015).
- [42] S. Shimomura, H. Muraō, S. Tsutsui, H. Nakao, A. Nakamura, M. Hedo, T. Nakama, and Y. Ōnuki, Lattice Modulation and Structural Phase Transition in the Antiferromagnet  $\text{EuAl}_4$ , J. Phys. Soc. Jpn. **88**, 014602 (2019).
- [43] T. Shang, Y. Xu, D. J. Gawryluk, J. Z. Ma, T. Shiroka, M. Shi, and E. Pomjakushina, Anomalous Hall resistivity and possible topological Hall effect in the  $\text{EuAl}_4$  antiferromagnet, Phys. Rev. B **103**, L020405 (2021).
- [44] K. Kaneko, T. Kawasaki, A. Nakamura, K. Munakata, A. Nakao, T. Hanashima, R. Kiyonagi, T. Ohhara, M. Hedo, T. Nakama, and Y. Ōnuki, Charge-Density-Wave Order and Multiple Magnetic Transitions in Divalent Europium Compound  $\text{EuAl}_4$ , J. Phys. Soc. Jpn. **90**, 064704 (2021).
- [45] X. Y. Zhu, H. Zhang, D. J. Gawryluk, Z. X. Zhen, B. C. Yu, S. L. Ju, W. Xie, D. M. Jiang, W. J. Cheng, Y. Xu, M. Shi, E. Pomjakushina, Q. F. Zhan, T. Shiroka, and T. Shang, Spin order and fluctuations in the  $\text{EuAl}_4$  and  $\text{EuGa}_4$  topological antiferromagnets: A  $\mu\text{SR}$  study, Phys. Rev. B **105**, 014423 (2022).
- [46] S. Hayami, Multiple Skyrmion Crystal Phases by Itinerant Frustration in Centrosymmetric Tetragonal Magnets, J. Phys. Soc. Jpn. **91**, 023705 (2022).
- [47] S. Hayami, Rectangular and square skyrmion crystals on a centrosymmetric square lattice with easy-axis anisotropy, Phys. Rev. B **105**, 174437 (2022).
- [48] See Supplemental Material at <http://xxxx> for details of experiments and analyses, which includes Refs. [49–52]
- [49] R. Daou, F. Weickert, M. Nicklas, F. Steglich, A. Haase and M. Doerr, High resolution magnetostriction measurements in pulsed magnetic fields using fiber Bragg gratings, Rev. Sci. Instrum. **81**, 033909 (2010).
- [50] A. Miyake, M. Gen, A. Ikeda, K. Miyake, Y. Shimizu, Y. J. Sato, D. Li, A. Nakamura, Y. Homma, F. Honda, J. Flouquet, M. Tokunaga, and D. Aoki, Magnetovolume Effect on the First-Order Metamagnetic Transition in  $\text{UTe}_2$ , J. Phys. Soc. Jpn. **91**, 063703 (2022).
- [51] M. Gen, A. Miyake, H. Yagiuchi, Y. Watanabe, A. Ikeda, Y. H. Matsuda, M. Tokunaga, T. Arima, and Y. Tokunaga, Enhancement of giant magnetoelectric effect in Ni-doped  $\text{CaBaCo}_4\text{O}_7$ , Phys. Rev. B **105**, 214412 (2022).
- [52] K. Shibata, J. Iwasaki, N. Kanazawa, S. Aizawa, T. Tanigaki, M. Shirai, T. Nakajima, M. Kubota, M. Kawasaki, H. S. Park, D. Shindo, N. Nagaosa, and Y. Tokura, Large anisotropic deformation of skyrmions in strained crystal, Nat. Nanotech. **10**, 589 (2015).
- [53] J. Prokleška, J. Vejpravová, V. Sechovský, Magnetostriction measurement of  $\text{GdRu}_2\text{Si}_2$  single crystal, J. Phys.: Conf. Ser. **51**, 028 (2006).
- [54] S. Ramakrishnan, S. R. Kotla, T. Rekiş, J.-K. Bao, C. Eisele, L. Noohinejad, M. Tolkiehn, C. Paulmann, B. Singh, R. Verma, B. Bag, R. Kulkarni, A. Thamizhavel, B. Singh, S. Ramakrishnan, and S. van Smaalen, Orthorhombic charge density wave on the tetragonal lattice of  $\text{EuAl}_4$ , IUCrJ **9**, 378 (2022).
- [55] M. Stavinoha, J. A. Cooley, S. G. Minasian, T. M. McQueen, S. M. Kauzlarich, C.-L. Huang, and E. Morosan, Charge density wave behavior and order-disorder in the antiferromagnetic metallic series  $\text{Eu}(\text{Ga}_{1-x}\text{Al}_x)_4$ , Phys. Rev. B **97**, 195146 (2018).
- [56] H. Zhang, X. Y. Zhu, Y. Xu, D. J. Gawryluk, W. Xie, S. L. Ju, M. Shi, T. Shiroka, Q. F. Zhan, E. Pomjakushina, and T. Shang, Giant magnetoresistance and topological Hall effect in the  $\text{EuGa}_4$  antiferromagnet, J. Phys.: Condens. Matter **34**, 034005 (2022).
- [57] J. M. Moya, S. Lei, E. M. Clements, C. S. Kengle, S. Sun, K. Allen, Q. Li, Y. Y. Peng, A. A. Husain, M. Mitrano, Matthew J. Krogstad, R. Osborn, A. B. Puthirath, S. Chi, L. Debeer-Schmitt, J. Gaudet, P. Abbamonte, J. W. Lynn, and E. Morosan, Incommensurate magnetic orders and topological Hall effect in the square-net centrosymmetric  $\text{EuGa}_2\text{Al}_2$  system, Phys. Rev. Materials **6**, 074201 (2022).
- [58] Z. Wang, Y. Su, S.-Z. Lin, and C. D. Batista, Meron, skyrmion, and vortex crystals in centrosymmetric tetragonal magnets, Phys. Rev. B **103**, 104408 (2021).
- [59] T. Takeuchi, M. Kakihana, M. Hedo, T. Nakama, and Y. -Onuki, Magnetic Field versus Temperature Phase Diagram for  $H \parallel [001]$  in the Trillium Lattice Antiferromagnet  $\text{EuPtSi}$ , J. Phys. Soc. Jpn. **88**, 053703 (2019).
- [60] S. Spachmann, A. Elghandour, M. Frontzek, W. Löser, and R. Klingeler, Magnetoelastic coupling and phases in the skyrmion lattice magnet  $\text{Gd}_2\text{PdSi}_3$  discovered by high-resolution dilatometry, Phys. Rev. B **103**, 184424 (2021).
- [61] It has not yet been experimentally revealed whether the  $a$  or  $b$  axis corresponds to the direction of the  $\mathbf{Q}$  vector in phases I and V, making the sign of  $dJ_1/dr$  unclear at this stage.

# Supplemental Material for “Rhombic skyrmion lattice coupled with orthorhombic structural distortion in $\text{EuAl}_4$ ”

Masaki Gen,<sup>1,2,\*</sup> Rina Takagi,<sup>2,3,4,5</sup> Yoshito Watanabe,<sup>1</sup> Naofumi Matsuyama,<sup>6</sup> Yoshimitsu Kohama,<sup>6</sup> Akihiko Ikeda,<sup>7</sup> Yoshichika Ōnuki,<sup>2</sup> Takashi Kurumaji,<sup>1</sup> Taka-hisa Arima,<sup>1,2</sup> and Shinichiro Seki<sup>2,3,4</sup>

<sup>1</sup>*Department of Advanced Materials Science, University of Tokyo, Kashiwa 277-8561, Japan*

<sup>2</sup>*RIKEN Center for Emergent Matter Science (CEMS), Wako 351-0198, Japan*

<sup>3</sup>*Institute of Engineering Innovation, University of Tokyo, Tokyo 113-0032, Japan*

<sup>4</sup>*Department of Applied Physics, University of Tokyo, Tokyo 113-8656, Japan*

<sup>5</sup>*PRESTO, Japan Science and Technology Agency (JST), Kawaguchi 332-0012, Japan*

<sup>6</sup>*Institute for Solid State Physics, University of Tokyo, Kashiwa 277-8581, Japan*

<sup>7</sup>*Department of Engineering Science, University of Electro-Communications, Chofu, Tokyo 182-8585, Japan*

This Supplemental Material includes contents as listed below:

- Sec. I. Sample preparation and experimental methods
- Sec. II. Raw data of magnetostriction curves measured along [100] for settings 1 and 2
- Sec. III. Additional experimental data for settings 1 and 2
- Sec. IV. FBG experiments on a nearly-detwinned crystal (setting 3)
- Sec. V. Possible slight orthorhombic structural distortion above  $T_{N3}$

## I. SAMPLE PREPARATION AND EXPERIMENTAL METHODS

Single crystals of  $\text{EuAl}_4$  were synthesized by the Al self-flux method as in Ref. [1]. The as-grown crystal was cut into the rectangular parallelepiped shape with the size of  $4 \times 3 \times 1.5 \text{ mm}^3$ . The magnetization was measured for  $H \parallel [001]$  using a commercial magnetometer (Magnetic Property Measurement System, Quantum Design).

The dilatometry measurements were performed by the fiber-Bragg-grating (FBG) method using an optical sensing instrument (Hyperion si155, LUNA), which monitors the Bragg-wavelength changes ( $\Delta\lambda/\lambda_0$ ) of the attached FBGs. For conversion from the experimental  $\Delta\lambda/\lambda_0$  to the sample-length change ( $\Delta L/L_0$ ), we use the linear relation  $\Delta\lambda/\lambda_0 = c(\Delta L/L_0)$  with a typical coupling parameter  $c = 0.76$  [2], which should be satisfied well below 50 K where the thermal expansion of background components are negligible. We confirm the validity of the above analysis in the previous work [3] and also in this study (see the main text). Our FBG technique is capable of high-precision detection of  $\Delta L/L_0$  with a resolution of  $\sim 10^{-7}$ , and allows simultaneous multi-axis measurements [3, 4]. The magnetic field was applied along [001] using a superconducting magnet (Spectromag, Oxford Instruments).

---

\* masaki.gen@riken.jp

## II. RAW DATA OF MAGNETOSTRICTION CURVES MEASURED ALONG [100] FOR SETTINGS 1 AND 2

Figure S1 shows the raw data of magnetostriction curves for  $H \parallel [001]$  measured along [100] at various temperatures: (a)  $(\Delta L/L_0)_1$  for setting 1 and (b)  $(\Delta L/L_0)_2$  for setting 2. As discussed in the main text,  $(\Delta L/L_0)_1$  and  $(\Delta L/L_0)_2$  were taken under different sample adhesion conditions. By using the relations  $\Delta a/a_0 = [p_2(\Delta L/L_0)_1 - p_1(\Delta L/L_0)_2]/(p_2 - p_1)$  and  $\Delta b/b_0 = [-(1 - p_2)(\Delta L/L_0)_1 + (1 - p_1)(\Delta L/L_0)_2]/(p_2 - p_1)$  with  $p_1 = 0.49$  and  $p_2 = 0.74$ , the field evolutions of  $\Delta a/a_0$  and  $\Delta b/b_0$  at the corresponding temperatures are obtained as shown in Figs. 3(a) and 3(b) in the main text.

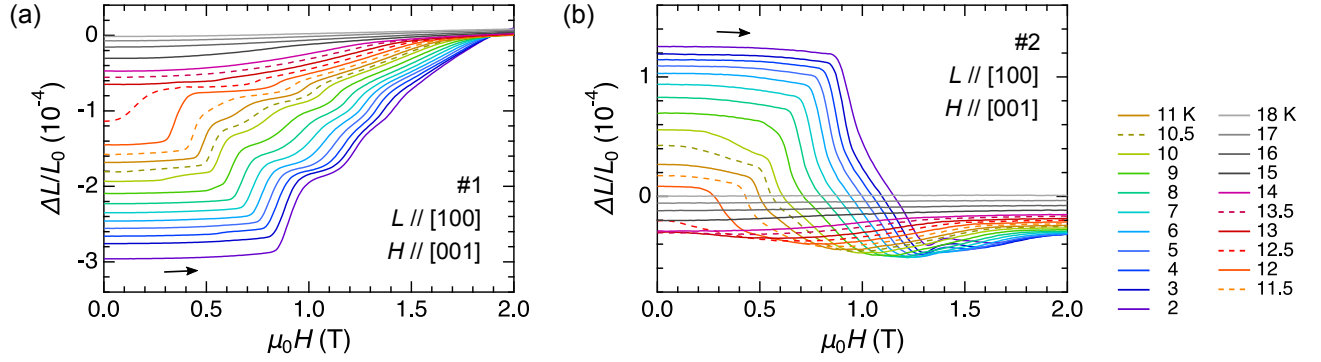


FIG. S1. Raw data of the observed magnetostriction curves for  $H \parallel [001]$  and  $\Delta L/L_0 \parallel [100]$  in  $\text{EuAl}_4$ : (a)  $(\Delta L/L_0)_1$  for setting 1 and (b)  $(\Delta L/L_0)_2$  for setting 2. The color scale of temperature is shown in the right side of (b).

## III. ADDITIONAL EXPERIMENTAL DATA FOR SETTINGS 1 AND 2

Figure S2(a) shows thermal expansion curves measured along [100] at constant magnetic fields for setting 1. These data were obtained after a series of magnetostriction measurements shown in Fig. S1(a). By comparing Figs. S1(a) and S2(a), it can be seen that  $\Delta L/L_0$  has the same value under certain temperature and magnetic field regardless of the sweep process. This ensures that the volume ratio of the magnetic domains never changes with scanning temperature as well as magnetic field.

Figure S2(b) shows magnetostriction curves measured along [100] at various temperatures for setting 2. These data were obtained on a different day (i.e., the probe was once taken out from the superconducting magnet and inserted again) without changing the sample setting in which the data shown in Fig. S2(b) were obtained, but they were surprisingly reproducible.

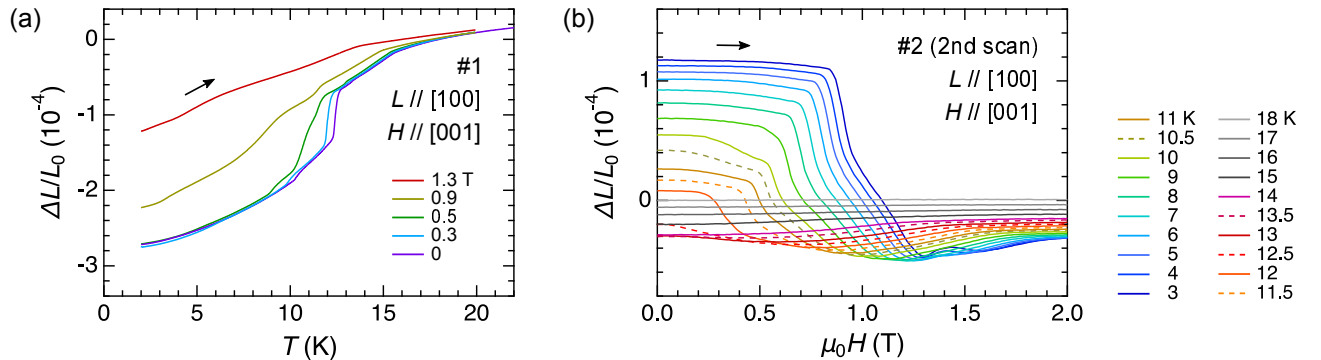


FIG. S2. (a) Thermal expansion measured along [100] at selected magnetic fields for  $H \parallel [001]$  in the warming process for setting 1. (b) Magnetostriction measured along [100] at selected temperatures for  $H \parallel [001]$  in the field-increasing process for setting 2.

#### IV. FBG EXPERIMENTS ON A NEARLY-DETWINNED CRYSTAL (SETTING 3)

In order to avoid the occurrence of magnetic domains and directly detect the lattice constant change  $\Delta b/b_0$  below  $T_{N3}$ , we performed the FBG experiments by applying the thermal stress on a  $\text{EuAl}_4$  single crystal. The experimental setting is illustrated in Fig. S3(a). The crystal was placed in a groove of the U-shaped block made of FRP (G-10), and facing (100) planes of the crystal were glued to the sides of the groove using Stycast1266. The optical fiber was adhered to the (001) plane along the bridging [100] direction. Since the thermal expansion coefficient of FRP is smaller than that of  $\text{EuAl}_4$ , the crystal should be tensile-strained along the bridging direction on cooling and could enter a nearly detwinned state below  $T_{N3}$ . Note that the similar way to apply the thermal stress has been previously employed in Ref. [5].

The observed thermal expansion profile in zero field is shown by a red line in Fig. S3(b). A large negative thermal expansion is observed below  $T_{N3}^* \approx 13.5$  K, reaching  $\Delta L/L_0 \approx 4 \times 10^{-4}$  at 2 K. By comparing with the x-ray data indicated by open circles [6], it is found that  $\sim 90\%$  of  $b$ -components contribute to the elongation of the FBG. Importantly, the original magnetostructural transition temperature  $T_{N3} = 12.2$  K shifts higher by more than 1 K, suggesting that the magnetism in  $\text{EuAl}_4$ , which should be strongly coupled to the lattice degrees of freedom, is sensitive to the uniaxial stress. Figure S3(c) shows the magnetostriction curves for  $H \parallel [001]$  measured along [100] at various temperatures on the strained crystal. These data are reasonably consistent with the estimated  $\Delta a/a_0$  and  $\Delta b/b_0$  shown in Figs. 3(a) and 3(b) in the main text. Note that we could not confirm the shift of the critical fields  $H_{c1} \sim H_{c4}$  from the original values at 2 K. It would be necessary to apply a stronger mechanical stress to control the stability of each SkL phase.

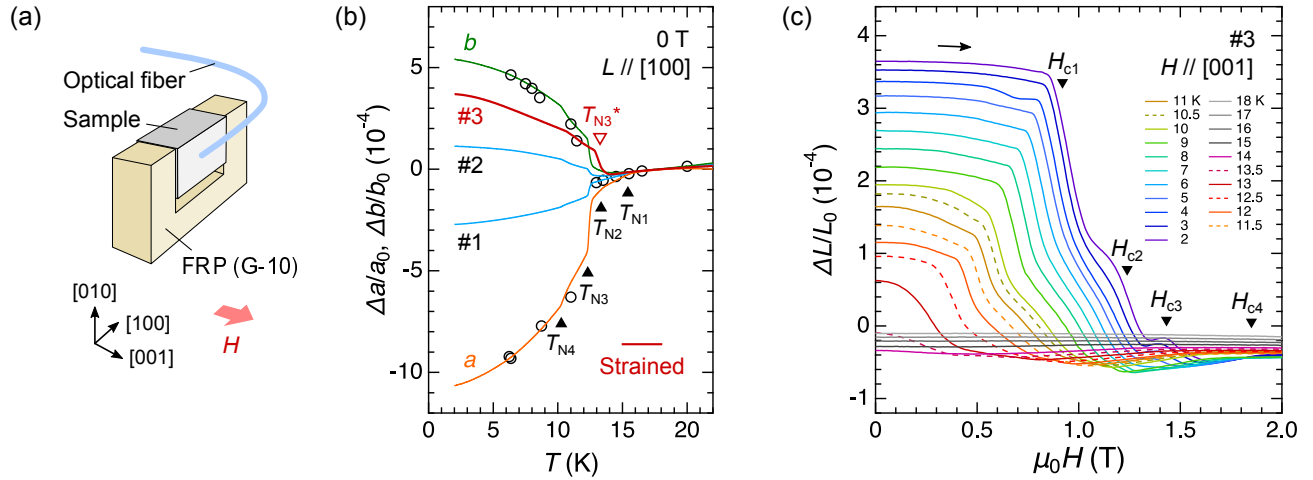


FIG. S3. (a) Schematic of the sample setting of the FBG experiments on a strained  $\text{EuAl}_4$  crystal. The tensile-strain should be applied along the measured direction at low temperatures. (b) Thermal expansion measured along [100] in zero field on unstrained (data #1 and #2 drawn by cyan lines) and strained crystals (data #3 drawn by red line). See also Fig. 2(b) in the main text. (c) Magnetostriction curves for  $H \parallel [001]$  and  $\Delta L/L_0 \parallel [100]$  on a strained crystal.

#### V. POSSIBLE SLIGHT ORTHORHOMBIC STRUCTURAL DISTORTION ABOVE $T_{N3}$

As for the estimation of the orthorhombic structural distortion  $\varepsilon \equiv (b - a)/a_0$  shown in Fig. 1(c), if we simply assume  $a_0 = b_0$  at 0 T and 18 K,  $\varepsilon$  turns to negative above  $\sim 1.7$  T at 2 K. This would not be intrinsic but presumably due to the missing incorporation of a tiny distortion at 0 T and 18 K, i.e.,  $a_0 < b_0$ , in our analysis. The recent x-ray study by Ramakrishnan *et al.* [7] suggested the presence of orthorhombic distortion as much as  $\sim 1 \times 10^{-4}$  within the  $ab$  plane below  $\sim 140$  K, where the charge density wave (CDW) with an incommensurate modulation along the  $c$  axis emerges [6, 8]. They argue that the in-plane lattice distortion is the  $B_{2g}$  type ( $Fmmm$  symmetry) rather than the  $B_{1g}$  type ( $Immm$  symmetry) [7]. However, we observe that  $\Delta b/b_0$  deviates from  $\Delta a/a_0$  between  $T_{N3}$  and  $T_{N1}$  [Fig. 2(b)], indicating the presence of a slight  $B_{1g}$ -type lattice distortion above  $T_{N3}$ . We infer that the both the  $B_{1g}$  and  $B_{2g}$  modes may be relevant in the CDW state, which would affect the estimation of  $\varepsilon$  especially in high-field or high-temperature sides. This ambiguity does not affect the conclusion of the present work.

- 
- [1] R. Takagi, N. Matsuyama, V. Ukleev, L. Yu, J. S. White, S. Francoual, J. R. L. Mardegan, S. Hayami, H. Saito, K. Kaneko, K. Ohishi, Y. Ōnuki, T. Arima, Y. Tokura, T. Nakajima, and S. Seki, *Nat. Commun.* **13**, 1472 (2022).
- [2] R. Daou, F. Weickert, M. Nicklas, F. Steglich, A. Haase and M. Doerr, High resolution magnetostriction measurements in pulsed magnetic fields using fiber Bragg gratings, *Rev. Sci. Instrum.* **81**, 033909 (2010).
- [3] A. Miyake, M. Gen, A. Ikeda, K. Miyake, Y. Shimizu, Y. J. Sato, D. Li, A. Nakamura, Y. Homma, F. Honda, J. Flouquet, M. Tokunaga, and D. Aoki, Magnetovolume Effect on the First-Order Metamagnetic Transition in  $UTe_2$ , *J. Phys. Soc. Jpn.* **91**, 063703 (2022).
- [4] M. Gen, A. Miyake, H. Yagiuchi, Y. Watanabe, A. Ikeda, Y. H. Matsuda, M. Tokunaga, T. Arima, and Y. Tokunaga, Enhancement of giant magnetoelectric effect in Ni-doped  $CaBaCo_4O_7$ , *Phys. Rev. B* **105**, 214412 (2022).
- [5] K. Shibata, J. Iwasaki, N. Kanazawa, S. Aizawa, T. Tanigaki, M. Shirai, T. Nakajima, M. Kubota, M. Kawasaki, H. S. Park, D. Shindo, N. Nagaosa, and Y. Tokura, Large anisotropic deformation of skyrmions in strained crystal, *Nat. Nanotech.* **10**, 589 (2015).
- [6] S. Shimomura, H. Murao, S. Tsutsui, H. Nakao, A. Nakamura, M. Hedo, T. Nakama, and Y. Ōnuki, Lattice Modulation and Structural Phase Transition in the Antiferromagnet  $EuAl_4$ , *J. Phys. Soc. Jpn.* **88**, 014602 (2019).
- [7] S. Ramakrishnan, S. R. Kotla, T. Rekiş, J.-K. Bao, C. Eisele, L. Noohinejad, M. Tolkiehn, C. Paulmann, B. Singh, R. Verma, B. Bag, R. Kulkarni, A. Thamizhavel, B. Singh, S. Ramakrishnan, and S. van Smaalen, Orthorhombic charge density wave on the tetragonal lattice of  $EuAl_4$ , *IUCrJ* **9**, 378 (2022).
- [8] A. Nakamura, T. Uejo, F. Honda, T. Takeuchi, H. Harima, E. Yamamoto, Y. Hag, K. Matsubayashi, Y. Uwatoko, M. Hedo, T. Nakama, and Y. Ōnuki, Transport and Magnetic Properties of  $EuAl_4$  and  $EuGa_4$ , *J. Phys. Soc. Jpn.* **84**, 124711 (2015).